

Resolving the Image of Gamma-ray Burst Afterglows with Gravitational Microlensing

B. Scott Gaudi¹

Institute for Advanced Study, Einstein Drive, Princeton, NJ 08540

Abraham Loeb

Harvard-Smithsonian CfA, 60 Garden Street, Cambridge, MA 02138

ABSTRACT

Microlensing of a gamma-ray burst afterglow by an intervening star can be used to infer the radial structure of the afterglow image. Near the peak of the microlensing event, the outer edge of the image is more highly magnified than its central region, whereas the situation is reversed at later times due to the rapid radial expansion of the image on the sky. Thus, the microlensed afterglow light curve can be inverted to recover the self-similar radial intensity profile of the afterglow image. We calculate the expected errors in the recovered intensity profile as a function of the number of resolution elements, under the assumption that the afterglow and microlensing event parameters are known. For a point-mass lens and uniform source, we derive a simple scaling relation between these parameters and the resultant errors. We find that the afterglow need not be monitored for its entire duration; rather, observations from the peak magnification time t_{peak} of the microlensing event until $7t_{\text{peak}}$ are sufficient to resolve the majority of the afterglow image. Thus, microlensing events can be alerted by relatively infrequent observations of afterglows. The relative intensity profile of a typical afterglow image can be measured with 10 resolution elements to an accuracy of 0 (1%) in the optical and 0 (10%) in the infrared, using 4m-class telescopes. Weak microlensing events with large impact parameters are more common; we estimate that for about 10% of all afterglows the image profile may be inverted to a fractional accuracy < 20% through frequent optical observations. We also calculate the effects of external shear due to the host galaxy or a binary companion, and contamination by background light from the host galaxy.

gamma-ray bursts { gravitational lensing

1. Introduction

Recent detections of afterglow emission in the X-ray, optical and radio has revolutionized gamma-ray burst (GRB) astronomy (for a recent review, see Kulkarni et al. 2000). The afterglow emission appears to be reasonably well-described by the reball model (Waxman, 1997a), in which a relativistically expanding shell of hot gas encounters an external quiescent medium. A blast wave is created, sweeping up the ambient material, and accelerating relativistic electrons which then emit synchrotron radiation (Paczynski & Rhoads, 1993; Mészáros & Rees, 1997). In this model, the spectral flux of the afterglow is a broken power-law function of frequency which evolves with time in a way that depends on the physical parameters of the reball and its surrounding medium, such as the total energy output of the GRB source, the collimation

¹Hubble Fellow

angle of the outflow, the ambient gas density, the fraction of the post shock energy which is converted into magnetic fields and accelerated electrons, and the energy distribution of the accelerated electrons (Sari, Piran, & Narayan, 1999). So far, observations of the afterglow spectrum over a wide range of frequencies and times was the primary method used to place constraints on these parameters (e.g. Wijers & Galama 1999; Panaitescu & Kumar 2001; Freedman & Waxman 1999). crude constraints on the size of the emitting region at late times were derived based on considerations involving synchrotron self-absorption (Katz & Piran, 1997) and radio scintillations due to the intervening interstellar medium of the Milky-Way galaxy (Goodman, 1997; Waxman, Kulkami, & Frail, 1998).

The afterglow image is predicted to appear as a thin ring on the sky (Waxman, 1997c; Sari, 1998; Panaitescu & Mészáros, 1998) at frequencies near or above the peak of the synchrotron emission (Granot, Piran & Sari, 1999a), but more like a uniform disk around or below the synchrotron self-absorption frequency (Granot, Piran & Sari, 1999b). In between breaks in the power-law spectrum of an afterglow, the contrast and width of this ring evolve self-similarly, i.e. the brightness profile maintains its shape as a function of radius when the latter is normalized by the expanding circular boundary of the image (Granot, Piran & Sari, 1999a). The self-similar brightness profile of the image changes only across spectral breaks (Granot & Loeb, 2001).

The outer radius of the image expands radially at an apparent superluminal speed of c , where c is the Lorentz factor of the emitting shock. The image occupies an angle of 1° relative to the center of the explosion due to relativistic beaming, and hence has a radius $R_s / r_{sh} = 1^\circ$, where r_{sh} is the shock radius. Geometric time delay implies that the observed time, $t / r_{sh} = 2$, and so $R_s / t = 2$. For an ambient density profile ρ / r^k , one gets $R_s / r_{sh} = (3k)^{1/2}$. Therefore, R_s / t with $(5-k) = 2(4-k)$. For a uniform ambient medium with $k = 0$ (Blandford & McKee, 1976), $R_s / t = 8$, while for a wind profile with $k = 2$ one gets $R_s / t = 4$. The predicted differences between the afterglow images in these two cases are typically small (Granot & Loeb, 2001).¹

By resolving the image of a GRB afterglow at different frequencies, one can obtain precious, new constraints on the reball model. As originally pointed out by Loeb & Perna (1998), after about one day, the angular size of a GRB ring is typically a micro-arcsecond (as), i.e. of the same order as the angular Einstein ring radius of a solar mass lens at cosmological distances,

$$E = \frac{4GM}{c^2 D} = 1.6 \frac{M}{M_\odot} \frac{D}{10^{28} \text{ cm}} \text{ as; } \quad (1)$$

where M is the lens mass, and $D_{os}D_{ol} = D_{ls}$, and D_{os} , D_{ol} and D_{ls} are the angular diameter distances between the observer-source, observer-lens, and lens-source, respectively. This fortuitous coincidence, along with the fact that the afterglow image expands superluminally, means that lensing by an intervening solar-mass star will produce a detectable deviation in the afterglow light curve with a duration suitable for intense monitoring. As the afterglow image expands, different parts of it sweep by the lens and get amplified. The differential magnification of the source image can be used to recover the radial structure of the afterglow image through a series of relative flux measurements (Loeb & Perna, 1998; Mao & Loeb, 2001; Granot & Loeb, 2001). The probability that a source at redshift $z = 2$ will have a projected angular distance less than the Einstein radius of any intervening star (the optical depth) is ~ 0.3 , where ρ is the cosmological density of stars in units of the critical density. The value of ρ is constrained to be $> 1\%$.

¹At very late times, of order months after the GRB trigger, the reball becomes non-relativistic. In this regime, the observer sees the entire reball which follows the Sedov-Taylor solution with $R_s / t = 5$.

based of the known populations of luminous (Fukugita, Hogan, & Peebles, 1998) and faint (Abdo et al., 2000) stars and $< 5\%$ based on Big-Bang nucleosynthesis. Hence, $\sim 1\%$ (Press & Gunn, 1973; Blaes & Webster, 1992; Kompaneets & Wambsganss, 2001), and roughly one out of a hundred afterglows should be strongly magnified (although all events may show weak magnification signals due to a star located at ten Einstein radii from their line-of-sight; see Mao & Loeb 2001).

Intense monitoring of lensing events could provide invaluable information about the nature of GRB afterglows. Recently, Gamovich, Loeb & Stanek (2000) interpreted the unusual optical afterglow light curve of GRB 000301C (Sagar et al., 2000; Rhoads & Fruchter, 2000) as being microlensed by an intervening

$0.5M_{\odot}$ star. The observed shape of the optical-infrared light curve constrained the source image to be a ring of fractional width $\sim 10\%$, in agreement with earlier theoretical predictions. Unfortunately, the optical-infrared photometry was too poor and coverage too sparse to actually measure the profile in detail, or uniquely constrain the microlensing interpretation through observations across spectral breaks (e.g. by comparing the magnification history in the radio to that in the optical).

The idea of using microlensing to study the images of gamma-ray burst afterglows is similar in spirit to the idea of using microlensing to resolve the atmospheres of stars in the Magellenic clouds and the Galactic bulge (Loeb & Sasselov, 1995; Valls-Gabaud, 1995; Sasselov, 1997; Heyrovsky, Sasselov, & Loeb, 2000); for a recent review, see Gould (2001). For background stars, the source radius stays constant and the resolution of the source occurs because the caustic structure of the lens sweeps over the face of the star due to the relative source-lens motion. However, for GRB afterglows the relative source-lens motion is negligible, and the resolution occurs as the image of the source itself is expanding and sweeping by the lens. Microlensing has been used to measure limb-darkening of the stars in the Small Magellanic Cloud and the Galactic bulge (Abdul et al., 1999a; Alonso et al., 2000; Abdul et al., 2000, 2001a) and also to measure the spatial variations of spectral lines across the face of two stars (Abdo et al., 1997; Castro et al., 2001; Abdul et al., 2001b; Heyrovsky, 2001). Gould & Gould (1999) considered the signal-to-noise requirements for resolving stellar atmospheres with microlensing. Our goal here is to apply similar considerations to GRB afterglows.

In this paper, we examine the observational constraints that can be obtained on afterglow images through a concerted monitoring effort of the GRB community in future microlensing events. Specifically, we determine the expected errors in the recovered intensity profile as a function of various parameters and input assumptions. This significance of this work is twofold: first, we show that the radial intensity profile of afterglows can be determined with fairly good accuracy ($\sim 10\%$) for reasonable expense of observational resources, and second, we present the effects of various assumptions on the error in the recovered intensity profile, in order to test the robustness of the conclusions and to provide guidelines for observers. In § 2 we present the formalism for microlensing of GRB afterglows. We describe the method for determining the expected errors in the recovered intensity profile in § 3, and apply it to a fiducial case in § 4.1. In § 4.2, we determine the effects of various input assumptions on the errors. Finally, we summarize the implications of our primary results in § 5.

For concreteness, we will primarily focus on the scaling laws of a spherical rebounce in a uniform medium, but derive a general scaling relation for the recovered errors in the relative intensity profile that is applicable for any power-law external density profile, $\rho \propto r^{-k}$. The two currently popular models, $k = 0$ (uniform medium) and $k = 2$ (stellar wind) yield qualitatively similar conclusions. We do not consider jetted outflows, although a collimated outflow of opening angle θ_{jet} would behave as if it is part of a spherical rebounce at early time as long as $\theta_{jet} \ll \theta_{jet}^*$ (Rhoads, 1997). We also assume that the afterglow flux exhibits a single power-law slope, which is appropriate if the observed frequency does not cross one of the several breaks in the afterglow spectrum (see Granot & Loeb 2001). Note that we do not assume any

specific model-dependent form for the intensity profile, i.e. we do not evaluate the errors on the coefficients of some parametric form for the profile. Rather, we evaluate the minimum attainable errors via direct inversion of the afterglow light curve.

2. Gamma-Ray Burst Afterglows and Microlensing

For a spherical rebill, the observer sees a circular source in age with an outer radius of angular size that evolves as,

$$s(t) = s_0 t_{\text{day}} ; \quad (2)$$

where s_0 is the angular size of the afterglow after 1 day, t_{day} is the observed time in days, and $s_0 = [5 - k]/[2(4 - k)]$ for an external medium with density profile $\rho \propto r^{-k}$. The angular size s_0 depends on the energy of the burst, the density of the ambient medium, and the redshift of the burst. For typical parameters, s_0 is of order 1 as. As long as an observed frequency, ν , does not cross any of the time-dependent spectralbreak frequencies, the afterglow flux at that frequency evolves as a power-law of time (e.g., Sari et al. 1999)

$$F(t) = F_0 s_0 t_{\text{day}} ; \quad (3)$$

where F_0 is the flux after 1 day. Granot & Loeb (2001) provide a comprehensive study of the predicted in age profile in the different spectral regimes.

Now assume that an intervening compact object lies at an angular distance b from the line-of-sight to the center of the afterglow. We may then normalize the angular radius of the afterglow in age in units of the Einstein radius of this object (Eq. 1),

$$R_s = R_0 t_{\text{day}} ; \quad (4)$$

where

$$R_0 = \frac{s_0}{R_E} ; \quad (5)$$

Since both s_0 and R_E are O(1 as) for typical parameters, R_0 is of order unity. The value of R_0 depends very weakly on the GRB energy output and the ambient density normalization, but is more sensitive to the lens mass and the source and lens redshifts (for $k = 0$, see Eqs. 2 & 3 in Granavich et al. 2000).

The magnification of an extended source is given by,

$$M(t) = \frac{\int_{R_s}^R d^2r s_0(r) I(t; r)}{\int_{R_s}^R d^2r I(t; r)} ; \quad (6)$$

where $s_0(r) = (r^2 + 2) = (r^2 + 4)$ is the point-source magnification at vector position r relative to the lens, and the integral is over the area of the source. For lensing of a uniform circular source of radius R_s by a single point mass with no external shear, the magnification obtains the value $M(t; R_s; b) = [r = R_s(t); b]$, where (Schneider, Ehlers & Falco, 1992; Witt & Mao, 1994),

$$M(t; b) = \frac{2}{r^2} \int_{b-r}^{b+r} dR \frac{R^2 + 2}{R^2 + 4} \arccos \frac{b^2 + R^2 - r^2}{2Rb} + H(r - b) \frac{r}{2} \frac{p}{(r - b)^2 + 4} ; \quad (7)$$

Here $H(x)$ is the step function and $b = R_E$ is the angular separation (impact parameter) between the source center and the lens in units of the Einstein ring radius.

For a uniform source (as applicable below the synchrotron self-absorption frequency; see Granot et al. 1999b and Granot & Loeb 2001), the magnification history by a point-mass lens is completely specified by two parameters: b and R_0 . Figure 1 shows the magnification as a function of time in days for $R_0 = 1$ and $b = 1$, and two density profiles, uniform ($\rho = 5=8$) and $\rho \propto r^{-2}$ ($\rho = 3=4$). At early times when the source radius is small, the magnification is roughly fixed at its point-source value $\mu(b) = \mu_0(b) = (b^2 + 2)/(b^2 + 4)$. The peak magnification occurs at a time t_{peak} when $R(t_{\text{peak}}) = b$, i.e. $t_{\text{peak}} = (b=R_0)^{1/2}$ days. The total flux from the afterglow is then by,

$$F_{\text{tot}}(t) = F_0(t; R; b) t_{\text{day}} + F_{\text{bg}}; \quad (8)$$

where we have allowed for flux F_{bg} from any unresolved sources not being lensed, e.g. the host galaxy of the GRB. Thus, in the simplest scenario the flux at a given frequency is a function of five parameters: F_0 , R , F_{bg} , R_0 , and b .

In order to illustrate how microlensing effectively resolves the image of the GRB afterglow, we plot in Figure 1 the fraction of F_{tot} contributed by five equal area annuli as a function of time assuming $b = 1$; $R_0 = 1$, and a uniform source. For $t < t_{\text{peak}}$, the annuli contribute roughly equal flux, and the source is not resolved. However, beginning at $t = t_{\text{peak}}$ different annuli obtain different weights and the lens differentially magnifies the source. The annulus that contributes most of the flux at a given time has a radius of $r_{\text{peak}} = r_0 t^{1/2}$ in units of R_0 , where r_0 is the radius of that annulus at $t = 1$ day. Defining the fractional radius $X = r/R_0$,

$$X_{\text{peak}} = \frac{t}{t_{\text{peak}}} : \quad (9)$$

From inspection of Figure 1 and equation (9), it is clear that the light curve need only be monitored from t_{peak} until $0.3 t_{\text{peak}}$ to resolve the outer 70% of the radial profile of the afterglow image.

3. Error Analysis

Consider an azimuthally symmetric afterglow divided into N_r annuli, with annulus i centered at radius r_i . We assume a self-similar behavior for which both the fractional radius X_i and the mean relative intensity $I(r_i) = I(t; r_i) = I(t)$ in each annulus are constants in time. The total flux from the afterglow is simply the sum of the fluxes from each annulus. The weight of each annulus is in turn the area of the image of each annulus of width r_i ,

$$(t; r_i) = [(t; r_i + r_i) (r_i + r_i)^2 - (t; r_i - r_i) (r_i - r_i)^2]; \quad (10)$$

times the mean intensity of that annulus. Converting equation (6) from an integral to a finite sum, the total flux is simply,

$$F_{\text{tot}}(t) = F_{\text{bg}} + \sum_i^{N_r} (t; r_i) I(r_i); \quad (11)$$

The coefficient one wishes to determine are the N_r relative intensities $I(r_i)$. These can be determined through inversion of the observed flux $F_{\text{tot}}(t)$ if F_{bg} , $I(t)$, and $(t; r_i)$ are known. The functions $I(t)$ and $(t; r_i)$ in turn depend on the parameters F_0 , b , and R_0 . Schematically, the inversion can be done as follows: and F_{bg} can be determined from the late-time ($t > t_{\text{peak}}$) behavior of the afterglow light curve. The unlensed flux of the afterglow could then be extrapolated back to $t = 1$ day, to determine F_0 . The offset between the lensed and unlensed flux at early times $t < t_{\text{peak}}$ then gives b . Finally, a

measurement of b combined with t_{peak} provides R_0 . Therefore, all the parameters necessary to invert equation (11) can ideally be determined without reference to the surface brightness distribution of the source image. In practice, of course, a global fit to all $5 + N_r$ parameters must be done simultaneously, and this will introduce correlations between the parameters $I(r_i)$ and $F_0, F_{\text{bg}}, R_0, b$, in turn increasing the errors on the measured values of $I(r_i)$. When computing the error bars on $I(r_i)$, we will assume that $F_0, F_{\text{bg}}, R_0, b$ are perfectly known, and so the errors we derive should be regarded as lower limits to the actual errors. However, we believe that our estimates are likely not considerably smaller than the actual errors, because a large number of data points at several different frequencies should help suppress some of the above correlations.

Now consider a series of flux measurements $F_{\text{tot}}(t_k)$ that are made at times t_k with errors ϵ_k , and that are fit to equation (11). The parameters of the fit are $I_i = I(r_i)$, and the variances in these parameters are $I_i = (C_{ii})^{1/2}$, where C_{ij} is the covariance matrix,

$$C = B^{-1}; \quad B_{ij} = \sum_k \frac{\partial F(t_k)}{\partial I_i} \frac{\partial F(t_k)}{\partial I_j}; \quad (12)$$

and $\partial F(t_k) = \partial I_i = I(t_k) \partial I_i$. The fractional errors are then $I_i = I_i = C_{ii}^{1/2} = I_i$. We assume Poisson-noise limited precision, so that $\epsilon_k = \sqrt{F(t_k)}$. Therefore, for a given set of assumptions about the microlensing event (b, R_0), the unlensed flux of the afterglow (F_0, F_{bg}) and the observational setup (duration of observations, telescope diameter, etc.), the covariance matrix C can be formed and the expected errors $I_i = I_i$ determined.

4. Results

4.1. Fiducial Scaling Relation

We now apply the formalism in § 3 to derive an approximate scaling relation for $I_i = I_i$. Rather than adopt specific (and therefore model dependent) forms for the afterglow flux F_0 , as a function of frequency and a specific observational setup, we will simply assume that the instrument being used collects photons per second from the unlensed afterglow at $t = 1$ day. In § 4.5, we will evaluate values of and thus the errors expected from a specific example of afterglow emission and observational setup. For our fiducial scenario, we assume a uniform source ($I_i = 1$), a negligible background flux ($F_{\text{bg}} = 0$), and that observations are made continuously from the burst until very late times $t = t_{\text{peak}}$. We also assume equal-area annuli, so that all bins have equal weight for a uniform source. We then calculate $I_i = I_i$ for a range of values of R_0, b , and N_r . Numerically, we find the following approximate scaling relation for the fractional errors in the recovered intensity profile,

$$\frac{I_i}{I_i} = 0.35 \frac{r_i}{R_s} \frac{5(1 - 8 + 3/2)}{1 \text{ s}^{-1}} \frac{1/2}{\frac{N_r}{10}} \frac{8/5}{R_0^{(1 - 2)/2}} b^{-2} : \quad (13)$$

Equation (13) is the primary result of this paper. We find that it predicts the expected errors to an accuracy of $\sim 5\%$ for most combinations of parameters. It is quite general, as it relies on only four assumptions about the afterglow, namely: (i) the unlensed flux of the afterglow is a power-law function of time, $F \propto t^{-5/3}$; (ii) the radius of the afterglow image scales as $R_s \propto t^{1/2}$; (iii) the image profile evolves self-similarly; and (iv) the afterglow image is circularly symmetric. The above equations can be used to determine the expected errors on the recovered intensity from observations performed with various instruments, apertures, and photon

frequencies of afterglow light curves of arbitrary fluxes and power-law indices. Because we have assumed that the observational precision is limited only by photon statistics, that there are no correlations with the other parameters (see the discussion in x 3), and that the measurements are continuous, equation (13) provides the minimum attainable error, at least for uniform sources and isolated lenses with no external shear. In the next section, we will relax some of the assumptions leading to this result in order to evaluate their effect on the expected errors. For the two cases of a uniform medium ($\gamma = 5=8$) and a stellar wind medium ($\gamma = 3=4$), the exponents in equation (13) are quite similar. Therefore, for the sake of simplicity, we will consider only the uniform medium case with $\gamma = 5=8$, in the discussion that follows.

Several of the terms in equation (13) can be derived analytically, simply by noting that, according to photon statistics, the errors should scale as $I_i = I_i / N^{1=2}$, where N is the number of photons collected. For example, the scaling with R_0 can be derived as follows: the time of the peak of the light curve scales as $t_{\text{peak}} / R_0^{1=}$. The unlensed flux at this time is $F(t_{\text{peak}}) / R_0^{1=}$. The magnification structure is independent of R_0 ; however, all times are scaled by $R_0^{1=}$, so the time over which photons can be collected scales as this factor. Thus the total error should scale as $(R_0^{1=} R_0^{1=})^{1=2} = R_0^{(1-1)=2}$, as found numerically. The scaling with the impact parameter b can be derived in a similar fashion, under the assumption that the peak magnification scales as b^{-1} . However, this is only strictly valid for $b \gg 1$. Therefore, the scaling $I_i = I_i / b^{1=2}$ in equation (13) is only approximate, and breaks down for $b \ll 1$. Numerically, we find that for $b = 4$, equation (13) predicts errors that are too small by $\sim 20\%$ for $r > 0.5R_s$ (the outer 70% of the area of the image). The exponent for the scaling with N_r is $8=5$, similar to that found by Gaudi & Gould (1999) for resolving the images of Galactic stars by microlensing. Naively, one might expect the prefactor in equation (13) to be considerably smaller: for $\gamma = 1$ and $b = 1$ the total number of photons collected is of order $N \sim 10^5$ ($\sim 1 \text{ s}^{-1}$) (with only a logarithmic dependence on the integration time during which the source is resolved). Divided over $N_r = 10$ bins, one might expect the error per bin to be $(N = N_r)^{1=2} \sim 1\%$ ($\sim 1 \text{ s}^{-1}$) $^{1=2}$, about an order of magnitude smaller than the $\sim 12\%$ ($\sim 1 \text{ s}^{-1}$) $^{1=2}$ predicted by equation (13) for a radius $r_i = 0.5R_s$. However, the errors increase with N_r faster than one would naively expect, and so the error in each bin is closer to $(N = N_r^{16=5})^{1=2} \sim 12\%$ ($\sim 1 \text{ s}^{-1}$) $^{1=2}$.

4.2. Effects of Changes in the Input Assumptions

4.2.1. Duration of Observations

The most severe simplification made in deriving equation (13) is the assumption of continuous measurement from the GRB trigger until long after the peak time t_{peak} . Since the optical depth for microlensing is $\sim 1\%$ b^{-2} , at least $100b^{-2}$ afterglows must be monitored to detect one that has impact parameter b . If it was truly necessary to monitor all of these afterglows continuously to recover the intensity profile accurately, this would represent an overwhelming observational burden. We therefore evaluate the errors expected under various assumptions about the starting time and the duration of the observations. We scale the starting time, t_{start} , and ending time, t_{end} , in terms of the peak time through the relation $(t-t_{\text{peak}})^{5=8}$, so that for given t_{start} and t_{end} , a fixed range of fractional radii, namely $X_{\text{min}} = \frac{1}{t_{\text{end}}}$ through $X_{\text{max}} = \frac{1}{t_{\text{start}}}$, are probed regardless of the values of R_0 and b (see Eq. 9). The top panel of Figure 2 shows the expected errors $I_i = I_i$ normalized to the fiducial errors in equation (13), for $(t_{\text{start}}, t_{\text{end}}) = (0.1, 100.0)$, corresponding to complete coverage of the microlensing event, and also for $t_{\text{start}} = 1$ (starting at the peak of the event) and various values of t_{end} . Note that here and throughout we plot $I_i = I_i$ as a function of $(r=R_s)^2$, because we assume bins of equal area (and hence equal weight for a

uniform source; see Eq. 10). Clearly observations before the peak of the event provide little information on the intensity profile. Moreover, the afterglow need only be monitored until $t = 7t_{\text{peak}}$ to resolve the outer two thirds of the source radius. The bottom panel of Figure 2 shows the expected errors when t_{start} is varied. Delaying observations even somewhat past the peak of the event will result in seriously degraded information.

We conclude that measurements from t_{peak} until $7t_{\text{peak}}$ will provide almost as much information as continuous measurements from the GRB trigger until late times. Since for typical parameters $t_{\text{peak}} = 1$ day, the afterglow need only be aggressively monitored for about six days. This suggests the following detection strategy for maximizing the number of lensed GRBs for which the intensity profile can be recovered. Since the sampling necessary to determine that the GRB is being microlensed is not as dense as that needed to recover the intensity profile, a large number of bursts can be monitored relatively infrequently from a global network of small telescopes. With real-time reduction, this network should be able to "alert" microlensing events before or near the peak time. Larger telescopes could then be used to densely sample the microlensed afterglow for the 6 days necessary to resolve the intensity profile. This is similar to the way Galactic microlensing observations are coordinated (Udalski et al., 1994; Loeb et al., 1996).

4.2.2. Realistic Intensity Profiles

In this section, we explore the effects of realistic intensity profiles on the resultant errors. The optical image of the afterglow is expected to be limb-brightened, because light from the edge of the afterglow suffers the longest time delay, and thus was emitted at earlier times when the reball was brighter (Waxman 1997c; Sari 1998; Panaiteescu & Mészáros 1998; Granot, Piran, & Sari 1999a,b). The contrast between the center and edge of the afterglow, as well as the sharpness of the cut-off in intensity at the outer edge of the afterglow, depends on the location of the observed frequency relative to the various spectral breaks in the broken power-law spectrum of afterglows (Granot et al. 1999a,b; Granot & Loeb 2001). The exact shape of the relative intensity profile will affect the shape of the light curve, as well as the resultant errors, with the errors expected to be larger near the center (where the relative intensity is smaller) than those calculated assuming a uniform source. Previous studies of microlensing (Loeb & Perna, 1998; Gamavich, Loeb & Stanek, 2000; Mao & Loeb, 2001) have parameterized the intensity profile as a uniform inner disk bounded by a uniform outer ring, with two parameters specifying the width W and contrast C of the ring. Of course, realistic intensity profiles do not exhibit such discontinuous features. The precise calculation of these profiles for the different spectral regimes of GRB afterglows is presented elsewhere (Granot & Loeb 2001). Here, we adopt a parameterized form for the relative intensity profile that captures the qualitative aspects of realistic profiles,

$$I(X) = I_0 \frac{h}{1 - c \frac{p}{1 - X^2} (1 - X^n)}; \quad (14)$$

where c and n are free parameters that define the shape of the profile, and I_0 is the normalization such that $\int_0^1 X dX I(X) = 1$. The index n defines the sharpness of the cut-off, and is roughly analogous to the width of the ring W . The coefficient c is related to the intensity at $X = 0$, and is roughly analogous to the contrast C . Note that for $c = 0$ and $n = 1$, this form reduces to a uniform source.

The top panel of Figure 3 shows $I(X)$ for a relatively gradual cut-off, $n = 20$, and various values of c . The bottom panel of Figure 3 shows the fractional errors $I = I_0$ relative to the fiducial errors for a uniform source in equation (13), given the image profiles shown in the top panel. Note that we normalize the variances I to the mean intensity I_0 rather than the intensity in that bin in order to avoid the fractional

errors $I = I$ blowing up when $I \rightarrow 0$ for large c . In general, the resultant errors are a factor ≤ 3 worse than than the uniform source case. In the most extreme example where $I(X) \rightarrow 0$ at the center of the image, the fractional errors can become quite large, but only for the innermost bin. For the outer half of the area of the image, the errors can be smaller than the uniform source case. Thus, in this case, measurements will result in a robust upper limit to the intensity at the center of the image, with a clear measurement for the outer part of the image. Therefore the ring-like structure of the image will be accurately recovered. We have also calculated, but do not show, the errors for the case of a sharp outer cut, $n = 500$. The results for this case are qualitatively and quantitatively similar to the results for $n = 20$. We conclude that realistic intensity profiles will not result in significantly increased errors relative to the uniform source estimate (Eq. 13), at least for the majority of the source area.

4.3. External Shear and Binary Lenses

We now consider more complicated models for the lens. The majority of lenses are likely to reside in galaxies, and a significant fraction of these may be in binary systems. Therefore, the assumption of an isolated single lens with no external shear used in the previous sections will not be valid. We therefore consider two other types of lenses: a single lens with external shear (Chang & Refsdal, 1979), and a binary lens (Schneider & Weiss, 1986). The former case is appropriate for a lens perturbed by either a wide binary companion or the potential of its host galaxy. The latter is appropriate for binary-lenses with separations $0 \leq 1$ or smaller. We compute the fractional errors in the recovered intensity profiles in the same manner as before, except that we must replace χ in equation (10) with the uniform-source magnification appropriate for the given lens model. We compute this magnification using the inverse ray-shooting method (see, e.g., Wambsganss 1997) as follows. The generalized lens equation for point masses and external shear can be expressed in complex coordinates on the plane of the sky as (Witt, 1990),

$$\frac{\chi^N}{\chi} = z + \sum_k \frac{z_k}{z_k - z}; \quad (15)$$

where χ is the complex source position, z is the complex image position, γ is the shear, m_k is the fractional mass of lens component k , and z_k is the position of this component. All distances are expressed in units of the angular Einstein ring of the combined mass of the system. For a single lens, $N = 1$, $\gamma = 1$, and $z_1 = 0$. For a binary-lens with no external shear, $\gamma = 0$, $N = 2$, the mass ratio is $q = z_1/z_2$, the dimensionless projected separation is $d = |z_1 - z_2|$, and we choose the origin to be the midpoint of the binary.

We sample the image plane uniformly and densely, solving for the source position using the appropriate form of equation (15). These positions are then binned in the source plane. The magnification of each bin is then just the surface density of rays in the image plane divided by the surface density of rays in the source plane. Since this procedure conserves flux, the resulting magnification map can then be convolved with a source of arbitrary size to compute the magnification of the extended source. We calculate magnification maps for $\gamma = 0.1, 0.2, 0.3$ and 0.4 , and one binary-lens configuration with $d = 0.8$ and $q = 1$. For the single lens with external shear, $N_r + 7$ parameters are needed to specify the light curve, namely: the N_r relative intensities I_i , plus F_0, γ, F_{bg}, R_0 , the shear γ , and two parameters that specify the position of the GRB with respect to the lens, which we denote as (x, y) . For the binary lens, we assume that $\gamma = 0$; however two additional parameters are needed to describe the topology of the lens, namely d and q , and so there are a total of $N_r + 8$ parameters. When calculating the errors on the parameters I_i , we will again assume that all other parameters are perfectly known. Here this assumption is somewhat justified than the single

lens case, not only because there are more parameters, but also because the effects of these parameters are in general not directly related to features in the light curve, and are likely to be subject to degeneracies or correlations, which will inflate the errors in the recovered I_i . Such degeneracies or correlations are known to inflate the errors in limb-darkening measurements of stars using Galactic binary-lens events, although not greatly so for well-measured light curves (Afonso et al., 2000; Abbott et al., 2001a). In the Galactic binary-lens case, determination of all parameter combinations that correspond to solutions to the observed light curve, and therefore identification of degeneracies and correlations between the parameters, is a formidable task (Mao & di Stefano, 1995; di Stefano & Perna, 1997; Abbott et al., 1999b). This is likely to also be true for GRB afterglows. A comprehensive study of parameter space is beyond the scope of this paper, and so we will simply assume that the binary lens parameters are known. This assumption facilitates comparison with the isolated single-lens case, which is the main purpose of our discussion here. We stress that the errors we derive under this assumption are almost certainly underestimates. In both the external shear and binary-lens case, we will assume a uniform afterglow image (see Mao & Loeb 2000 for other examples).

In Figure 4 we show the magnification light curves for the case of a single lens with external shear along the x-axis of magnitudes $\gamma = 0; 0.1; 0.2; 0.3$, and 0.4 , both for a source centered on the x-axis of the lens, $(x; y) = (1; 0)$, and a source centered on the y-axis of the lens $(x; y) = (0; 1)$. Note that the caustics are most highly elongated along the x-axis, and thus for a given γ , light curves where the source is centered on the x-axis should show more dramatic deviations from the $\gamma = 0$ case than for sources centered on the y-axis (Mao & Loeb 2000). Figure 5 shows the resultant errors relative to the fiducial error estimate in equation (13). In general, sources centered on the x-axis show more dramatic variations in the expected errors than sources centered on the y-axis. In all cases the fractional errors are within a factor of 2 of the $\gamma = 0$ expectation. Thus, at least for modest values of $\gamma \leq 0.4$, we conclude that an external shear will not result in significantly inflated errors.

In Figure 6, we show the magnification as a function of time for the binary lens with $d = 0.8$ and $q = 1$, and a source centered at $(x; y) = (-0.16; 1)$. We also show the fraction of total flux contributed by five equal-area bins as a function of time. For times $t > 1$ day, the light curves resemble that for a single lens (compare with Figure 1), as the annuli become comparable to or larger than the caustic features. The bottom panel of Figure 6 shows the resultant errors relative to the fiducial single-lens case. Again, the errors differ by less than a factor of 2 from the fiducial estimate in equation (13).

4.4. Finite Unresolved Flux

Observed afterglows often show evidence for a flattening of the light curve to a constant flux at late times. This is usually interpreted as due to unresolved flux from the host galaxy of the GRB. Even if the flux from the host galaxy is small, the sky background will eventually dominate over that of the afterglow. In other words, it is inevitable that $F(t) < F_{bg}$ at late times. For ground-based infrared observations, the background flux is likely to be larger than the afterglow flux at all relevant times. A finite background flux will increase the errors on the recovered parameters I_i , and preferentially so for smaller radii, since the information on smaller radii comes at later times, when the background is more significant. We explore this effect by introducing a background flux which amounts to some fraction of $F_{,0}$ for the afterglow. Figure 7 shows the expected fractional errors on the recovered intensity profile relative to the fiducial value in equation (13), assuming a power-law flux index of $\gamma = 1$ for the afterglow, for relative background fluxes of $F_{bg}/F_{,0} = 0.01; 0.1; 0.4; 1.0; 2.5$, and 10.0 . At optical-infrared frequencies, this corresponds to a

background of magnitude 5;2.5;1;0; 1; 2.5 relative to the (unlensed) afterglow at 1 day. As expected, the errors generally increase as the background flux increases, especially for smaller radii. However, unless the background flux is higher than $F_{\text{c},0}$, the expected errors are ~ 3 times greater than the fiducial estimate. In other words, for optical frequencies, the background flux should not compromise the measurement of the intensity profile. However, for, e.g., ground-based observations in the near-infrared, where the sky background can be many magnitudes brighter than the afterglow flux at 1 day, the accuracy with which the intensity profile can be measured will considerably larger than the fiducial estimate (Eq. 13). Thus space-based near-infrared observations would improve the accuracy of the recovered intensity profile.

4.5. A Worked Example

As discussed in § 4.1, the results we have presented so far are quite general. We now estimate the errors expected under realistic observational conditions and a realistic model. To do so, we make estimates of the various terms in equation (13) by adopting the parameters for the observed afterglow of GRB 000301C. Gamovich, Loeb & Stanek (2000) fit the optical and infrared photometry of GRB 000301C to double power-law flux decline magnified by the simple microlensing model of Loeb & Perna (1998). They find best-fit parameters of $\alpha_1 = 1.1$ and $\alpha_2 = 2.9$ for the power-law flux indices, similar to the values found originally by Sagar et al. (2000) without including the microlensing model. For simplicity, we ignore the break, and simply adopt a single power-law of slope $\alpha = 1.1$. We adopt the best-fit microlensing parameters for the entire dataset of $R_0 = 0.49$ and $b = 1.04$. Finally, we extrapolate by eye the unlensed flux of the afterglow back to $t = 1$ day for the U;B;V;R;I;J and K-bands. Table 1 shows the demagnified, extrapolated magnitudes at $t = 1$ day of the afterglow of GRB 000301C, along with the assumed sky brightness, and $\phi = A_T$, the number of photons per second per square meter of collecting telescope area A_T . Note that, for $R_0 = 0.49$ and $b = 1.04$, the peak of the microlensing event (for a uniform source) occurs at $t_{\text{peak}} = (b/R_0)^{1/5} \approx 3$ days. We calculate the expected errors $\Delta I = I - I_{\text{true}}$ assuming a 4-m telescope, a seeing of $1''$, a uniform source, and observations between the peak, $t = t_{\text{peak}} = 3$ days and $t' = 9t_{\text{peak}} = 30$ days. We adopt a uniform source in order to provide a model-independent estimate of the fractional errors expected for realistic observing conditions. Image profiles in the optical and infrared are unlikely to be well-represented by a uniform source (Granot & Loeb, 2001), however this will not affect the errors in the recovered profile by more than a factor of ~ 3 (see § 4.2.2). The results are shown in Figure 8. For observations in the optical, the relative intensity profile can be recovered accurately, $\Delta I/I \lesssim 3\%$. For observations in the infrared, where the sky background is dominant, the expected errors are $\sim 10\%$. Although we do not specifically consider other wavelengths here, we note that radio afterglows peak later and last longer than afterglows at shorter wavelengths (Kulkarni et al. 2000 and references therein). This, combined with the lower energy of the photons, implies that the photon flux at a given time is larger in the radio than in the optical. At sufficiently high radio frequencies where the effect of scintillations is sub-dominant, radio observations may provide more accurate measurements of the afterglow image. Since the afterglow image is expected to be different at radio frequencies (Granot & Loeb, 2001), we advocate performing measurements over as wide a range of frequencies as possible.

Given that the fraction of afterglows that exhibit microlensing events with impact parameter b scales as b^2 , it is interesting to consider what kind of errors one would expect for the specific example of GRB 000301C considered above, but with larger impact parameters. We therefore repeat the calculation above with the same parameters, except we now vary the impact parameter. Specifically, we consider $b = 1; 2; 3; 4$, and 5, as would be expected in 1%; 4%; 9%; 16%, and 25% of all GRB afterglows. In Figure 9 we show

the results for the U-band (where the background is the smallest), assuming that observations are taken from peak, $t = t_{\text{peak}} = 3b^{5/8}$ days until $t' = 9t_{\text{peak}} = 30b^{5/8}$ days.

For $b = 3$, the fractional errors in the recovered intensity profile are $\leq 10\%$ for the majority of the area of the image. Thus, it should be possible to recover the intensity profile to an accuracy of $\leq 20\%$ for $\leq 10\%$ of all afterglows. To test the robustness of this conclusion, we also show in Figure 9 the results for the $b = 3$ case, but considering a band with larger background flux (R-band), and also a non-zero external shear ($\gamma = 0.2$ with source on the shear axis). We find that the error is not greatly inflated, $I = I \leq 20\%$. Of course, these results assume that the afterglow can be monitored for many months after the peak of the microlensing event. Practical aspects aside, such monitoring may not be possible even in principle in those cases where the emission is due to a highly collimated jet. Such afterglows will eventually exhibit breaks in the light curve and changes in the image structure when the Lorentz factor of the reball falls below the inverse of the opening angle of the jet. In this case, the errors on the annuli centered at smaller radii would be inflated (see x4.2.1). Additional deviations from our results may occur as the reball decelerates to non-relativistic speeds (Mao & Loeb, 2001).

5. Conclusions

Microlensing offers a unique method for probing the dynamics of GRB reballs. As the GRB afterglow image expands, it is differentially magnified by the lens. Different annuli of the image are resolved as they cross the lens position at different times. Thus the light curve of the afterglow during the microlensing event can be inverted to obtain the radial intensity profile $I(X)$, where $X = r/R_s$ is the fractional radius of the circular image. We developed the formalism necessary to calculate the expected fractional errors on the recovered intensity profile $I = I$ under a set of four general assumptions: (1) the unlensed flux of the afterglow is a power-law function of time, (2) the radius of the afterglow image scales as a power-law of time R_s / t , (3) the afterglow image is circularly symmetric, and (4) the intensity profile is self-similar, i.e. $I(X)$ is independent of time. All of these assumptions are rather general predictions of afterglow models, and hence not very restrictive.

Assuming continuous observations, uniform sources, single lenses, and zero background flux, we find that the expected errors follow a general scaling relation (Eq. 13) in terms of the afterglow flux, afterglow radius in units of the Einstein radius, the angular separation between the afterglow and the lens, and the number of resolution elements in the recovered intensity profile.

We have tested the accuracy of this relation by, in turn, relaxing the assumptions of continuous observations, uniform sources, single lenses, and zero background flux. We find that, for reasonable choices of the relevant parameters, none of these refinements changes the expected errors by more than a factor of 3. Therefore, the fiducial scaling relation is fairly robust.

Notably, we have found that observations starting at the peak t_{peak} of the microlensing event and ending at $7t_{\text{peak}}$ result in almost the same accuracy as measurements of the entire afterglow. Therefore, one can monitor frequently only those afterglows that are significantly microlensed by 'alerting' to these events before they reach their peak.

Finally, we calculated the errors expected for observations in the near-infrared and optical regimes of a specific example. Adopting the observed and inferred parameters for the (possibly) microlensed optical/infrared afterglow of GRB 000301C, we find that the relative intensity profile can typically be

measured with a resolution of 10 and accuracy of 0 (1%) in the optical and 0 (10%) in the infrared using 4m-class telescopes. Fluctuations in the light curve due to inhomogeneities in the ambient gas distribution are typically small and should not compromise this precision (Wang & Loeb, 2000; Halpern et al., 2000).

These results are encouraging. Errors of 1% would likely provide very stringent constraints on afterglow models, and even errors of 10% would be interesting (see Fig. 2 in Granot & Loeb 2001). Errors of the latter magnitude can be obtained from events with larger impact parameters. For the specific afterglow parameters adopted above, we find errors of $I=I$ 6%; 10%; 20% in the U-band for impact parameters in units of E of $b=2, 3$ and 4. Since the number of expected events scales as b^2 , this implies that interesting results might be obtained for a significant sample of afterglows. The forthcoming Swift satellite² could provide hundreds of afterglow targets per year. A network of 1m-class telescopes similar to that used in gravitational microlensing searches of the Local Group (Albrow et al., 1998; Rhee et al., 1999) would provide an ideal method for "alerting" the community to microlensed afterglows, which could in turn be intensively monitored to provide information about the structure of the afterglow in age. Although this represents a considerable expenditure of resources, the information gained would be invaluable, and furthermore cannot be currently acquired by any other method.

Acknowledgments

We thank Andrei Gruzinov for helpful discussions. This work was supported in part (for SG) by NASA through a Hubble Fellowship grant from the Space Telescope Science Institute, which is operated by the Association of Universities for Research in Astronomy, Inc., under NASA contract NAS5-26555, and (for AL) by grants from the Israel-US BSF (BSF-9800343), NSF (AST-9900877), and NASA (NAG 5-7039).

References

- Afonso, C., et al. 2000, *ApJ*, 532, 340
- Albrow, M., et al. 1998, *ApJ*, 509, 687
- Albrow, M., et al. 1999a, *ApJ*, 522, 1011
- Albrow, M., et al. 1999b, *ApJ*, 522, 1022
- Albrow, M., et al. 2000, *ApJ*, 534, 894
- Albrow, M., et al. 2001a, *ApJ*, 549, 000
- Albrow, M., et al. 2001b, *ApJL*, submitted (astro-ph/0011380)
- Alcock, C., et al. 1996, *ApJ*, 463, L67
- Alcock, C., et al. 1997, *ApJ*, 491, 436
- Alcock, C. et al. 2000, *ApJ*, 542, 281
- Blaes, O. M., & Webster, R. L. 1992, *ApJ*, 391, L63

²Planned for launch in 2003; see <http://swift.sonoma.edu/>

Blandford, R. D., & McKee, C. F. 1976, *Phys. Fluids*, 19, 1130

Castro, S. M., Pogge, R. W., Rich, R. M., Depoy, D. L., & Gould, A. 2001, *ApJL*, in press

Chang, K., & Refsdal, S. 1979, *Nature*, 282, 561

di Stefano, R., & Perna, R. 1997, *ApJ*, 488, 55

Fruchter, A. S., et al. 1999, *ApJ*, 516, 683

Frail, D. A., et al. 1997, *Nature*, 389, 261

Freedman, D. L., & Warmann, E. 1999, *ApJ*, submitted (astro-ph/9912214)

Fukugita, M., Hogan, C. J., & Peebles, P. J. E. 1998, *ApJ*, 503, 518

Gaudi, B. S., & Gould, A. 1999, *ApJ*, 513, 619

Garnavich, P. M., Loeb, A., & Stanek, K. Z. 2000, *ApJ*, 544, L11

Goodman, J. 1997, *New Astronomy*, 2, 449

Gould, A. 2001, *PA SP*, in preparation

Granot, J., & Loeb, A. 2001, *ApJL*, submitted (astro-ph/0101234)

Granot, J., Piran, T., & Sari, R. 1999a, *ApJ*, 513, 679

Granot, J., Piran, T., & Sari, R. 1999b, *ApJ*, 527, 236

Halpern, J., et al. 2000, *ApJ*, 543, 697

Heyrovsky, D. 2001, *ApJ*, submitted

Heyrovsky, D., Sasselov, D., & Loeb, A. 2000, *ApJ*, 543, 406

Katz, J., & Piran, T. 1997, *ApJ*, 490, 772

Koopmans, L. V. E., & Lambas, J. 2001, *MNRAS*, submitted (astro-ph/0011029)

Kulkami, S. R., et al. 2000, in *AIPC Conf. Proc.*, Gamma-Ray Bursts: 5th Huntsville Symposium, ed. R. M. Kippen, R. S. M. Mallozzi, & G. J. Fishman (New York: AIP)

Loeb, A., & Perna, R. 1998, *ApJ*, 495, 597

Loeb, A., & Sasselov, D. 1995, *ApJ*, 449, L33

Mao, S., & di Stefano, R. 1995, *ApJ*, 440, 22

Mao, S., & Loeb, A. 2001, *ApJ*, in press (astro-ph/0010029)

Mészáros, P., & Rees, M. J. 1997, *ApJ*, 476, 232

Paczynski, B., & Rhoads, J. E. 1993, *ApJ*, 418, L5

Panaitescu, A., & Kumar, P. 2001, *ApJ*, submitted (astro-ph/0010257)

Panaiteescu, A., & Mészáros, P. 1998, 493, L31

Péan, E., et al. 1998, ApJ, 492, L103

Press, W. H., & Gunn, J.E. 1973, ApJ, 185, 397

Rhie, S.H., Becker, A.C., Bennett, D.P., Fragile, P.C., Johnson, B.R., King, L.J., Peterson, B.A., & Quinn, J. 1999, ApJ, 522, 1037

Rhoads, J.E. 1997, ApJ, 487, L1

Rhoads, J., & Fruchter, A.S. 2000, ApJ, in press

Sagar, R., Mohan, V., Pandey, S.B., Pandey, A.K., Stalin, C.S., & Tirado, A.J. 2000, BASI, 28, 499

Sasselov, D. 1997, in Variable Stars and the Astrophysical Returns of Microlensing Surveys, ed. R. Ferlet, J.-P. Maillard, & B. Rabin (Gif-sur-Yvette: Editions Frontières), 141

Sari, R. 1998, ApJ, 494, L49

Sari, R., Piran, T., & Narayan, R. 1998, ApJ, 497, L17

Schneider, P., & Weiss, A. 1986, 164, 237

Schneider, P., Ehlers, J., & Falco, E.E. 1992, Gravitational Lenses (Heidelberg: Springer), p. 313

Udalski, A., Szymański, M., Kaluzny, J., Kubiać, M., Matese, M., Krzeminski, W., & Paczynski, B. 1994, A&A, 44, 227

Valls-Gabaud, D. 1995, in Large Scale Structure of the Universe, ed. J.P. Mucket, S.G. Ottobre, & V.M. Uller (Singapore: World Scientific), 326

Wang, X., & Loeb, A. 2000, ApJ, 535, 788

Wijers, R.A.M.J., & Galama, T.J. 1999, ApJ, 523, 177

Witt, H. 1990, A&A, 236, 311

Witt, H.J., & Mao, S. 1994, ApJ, 430, 505

Wambsganss, J. 1997, MNRAS, 284, 172

Waxman, E. 1997a, ApJ, 485, L5

Waxman, E. 1997b, ApJ, 489, L33

Waxman, E. 1997c, ApJ, 491, L19

Waxman, E., Kulkami, S.R., & Frail, D.A. 1998, ApJ, 497, 288

Filter	Apparent Magnitude ¹	sky (mag asec ⁻²)	=A _T ² (s ⁻¹ m ⁻²)
U	20.1	22.8	43
B	20.6	22.5	77
V	20.1	21.5	78
R	19.7	20.8	130
I	19.3	19.3	128
J	18.3	15.9	194
K	16.8	13.7	540

Table 1 Adopted fluxes for GRB 000301C.

¹Demagnified apparent magnitude of GRB 000301C extrapolated to 1 day after the burst.²Number of photons per second per square meter of collecting area A_T.

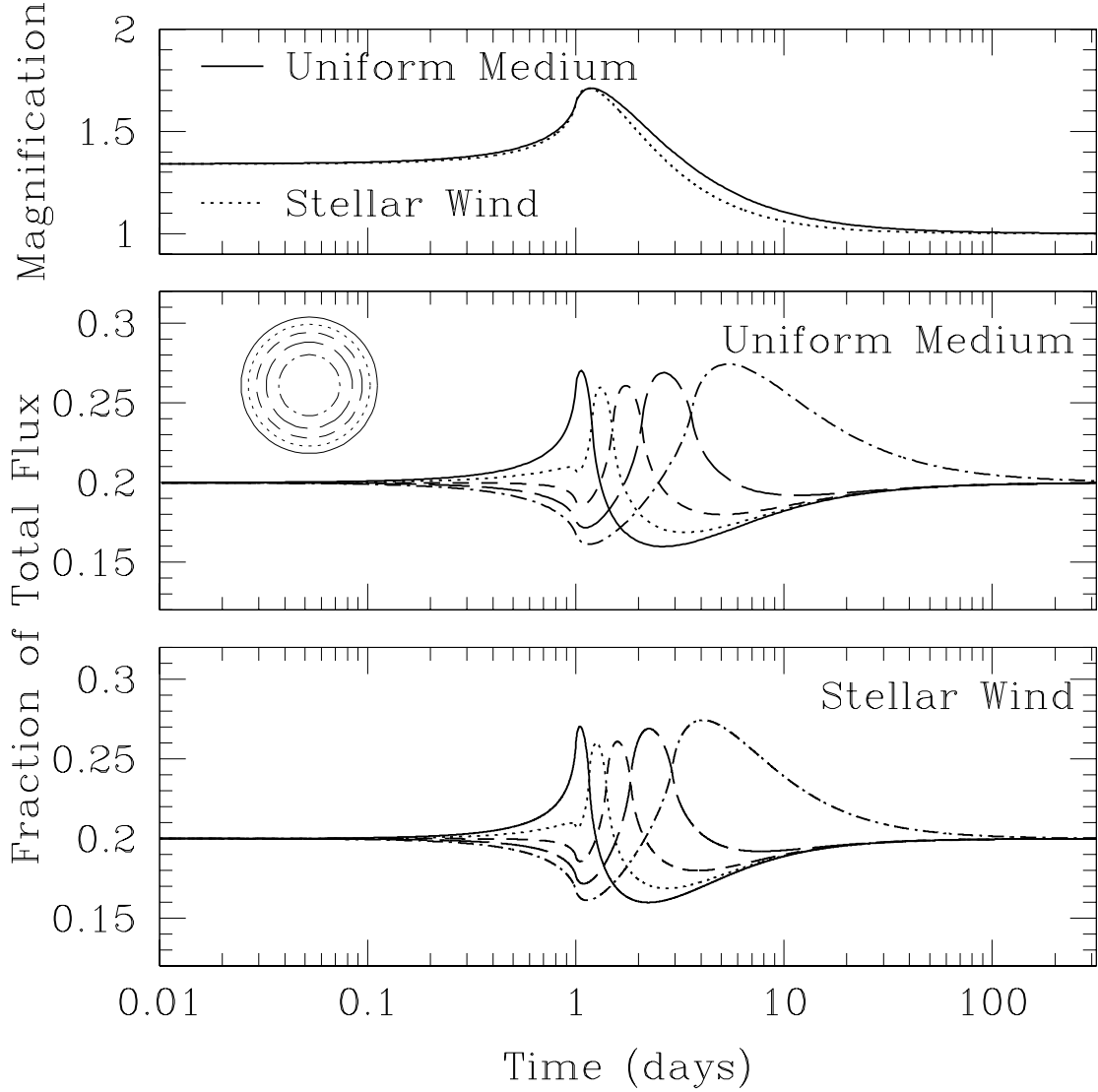


Fig. 1. The top panel shows the magnification as a function of time for a uniform source with radius $R_0 = 1$ at $t = 1$ day and an impact parameter $b = 1$, assuming a uniform external medium (solid line, \propto constant) and a medium such as that created by a stellar wind (dotted line, $\propto 1/r^2$). The middle panel shows the fraction of total flux contributed by five equal area annuli as a function of time in days for the uniform external medium, while the lower panel shows the same but for the stellar wind medium.

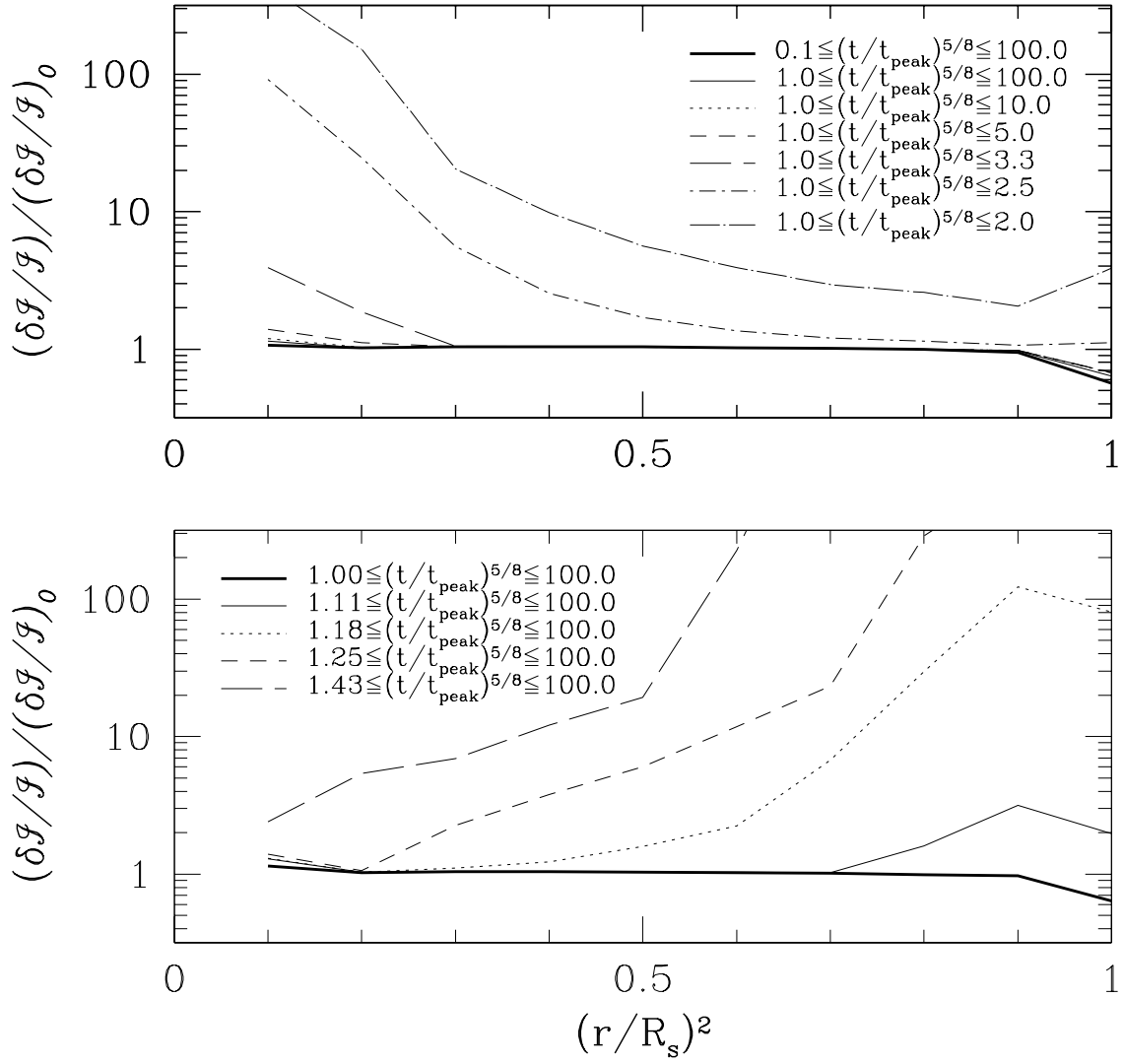


Fig. 2. Both panels show the fractional error in the recovered intensity profile $I=I/I_0$ normalized to that given by the fiducial error $(I=I)_0$ given by the scaling relation in equation (13), as a function of the square of the normalized radius $X = r=R_s$ of the afterglow. Each line shows under various assumptions of the beginning and duration of observations relative to the time t_{peak} of the peak of the microlensing event. Top Panel: Varying the end of observations relative to t_{peak} . Bottom Panel: Varying the beginning of observations relative to t_{peak} .

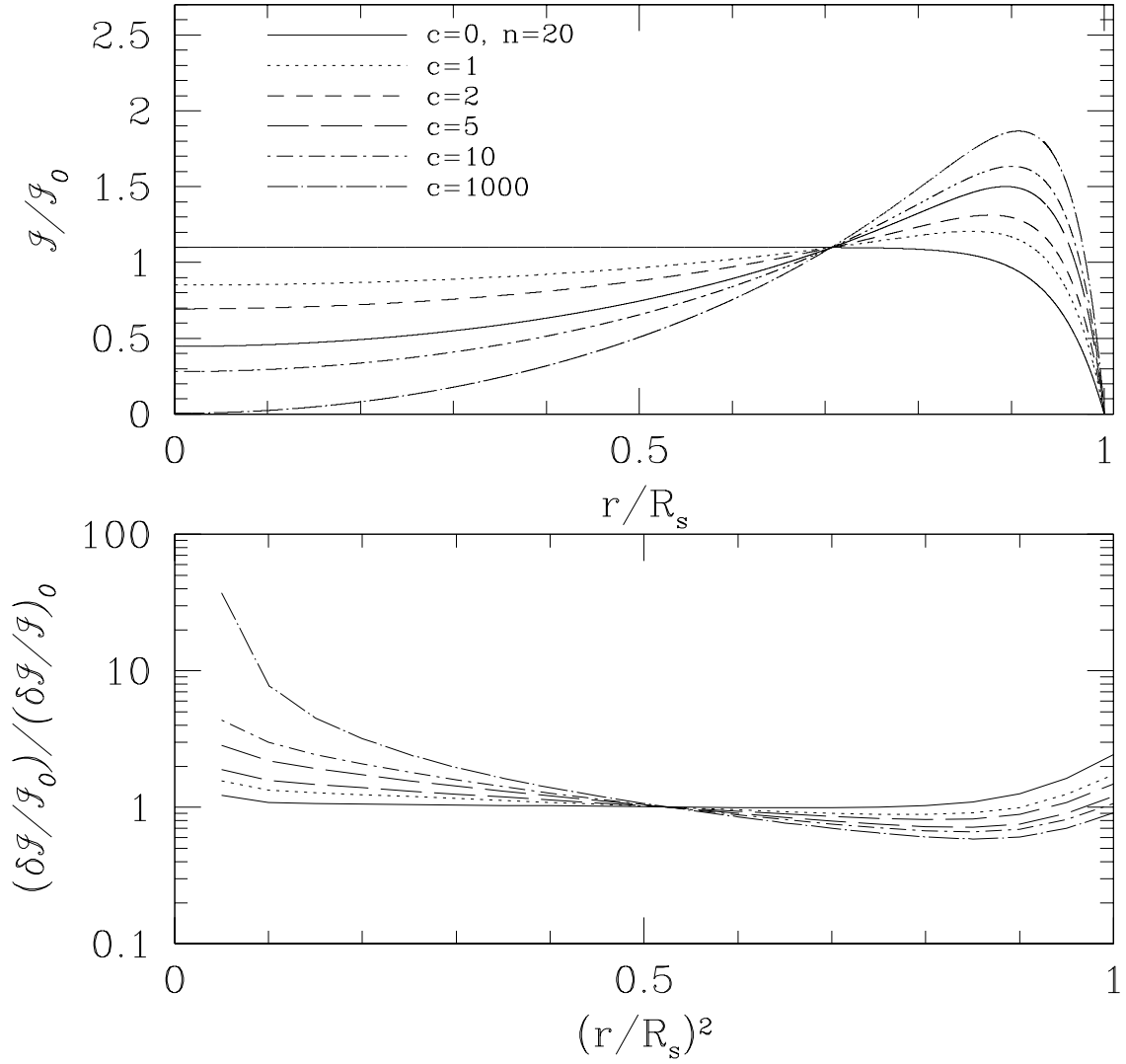


Fig. 3. | Top Panel: The normalized intensity profile $I(r)/I_0$ of the source as a function of the normalized radius $X = r/R_s$, assuming a cut-off parameter $n = 20$ and for several different values of the parameter c (see text and equation (14) for details). Bottom Panel: The fractional error in the recovered intensity profile I/I_0 normalized to that given by the fiducial error $(I/I_0)_0$ given by the scaling relation in equation (13), as a function of the square of the normalized radius of the afterglow, for the intensity profiles shown in the top panel.

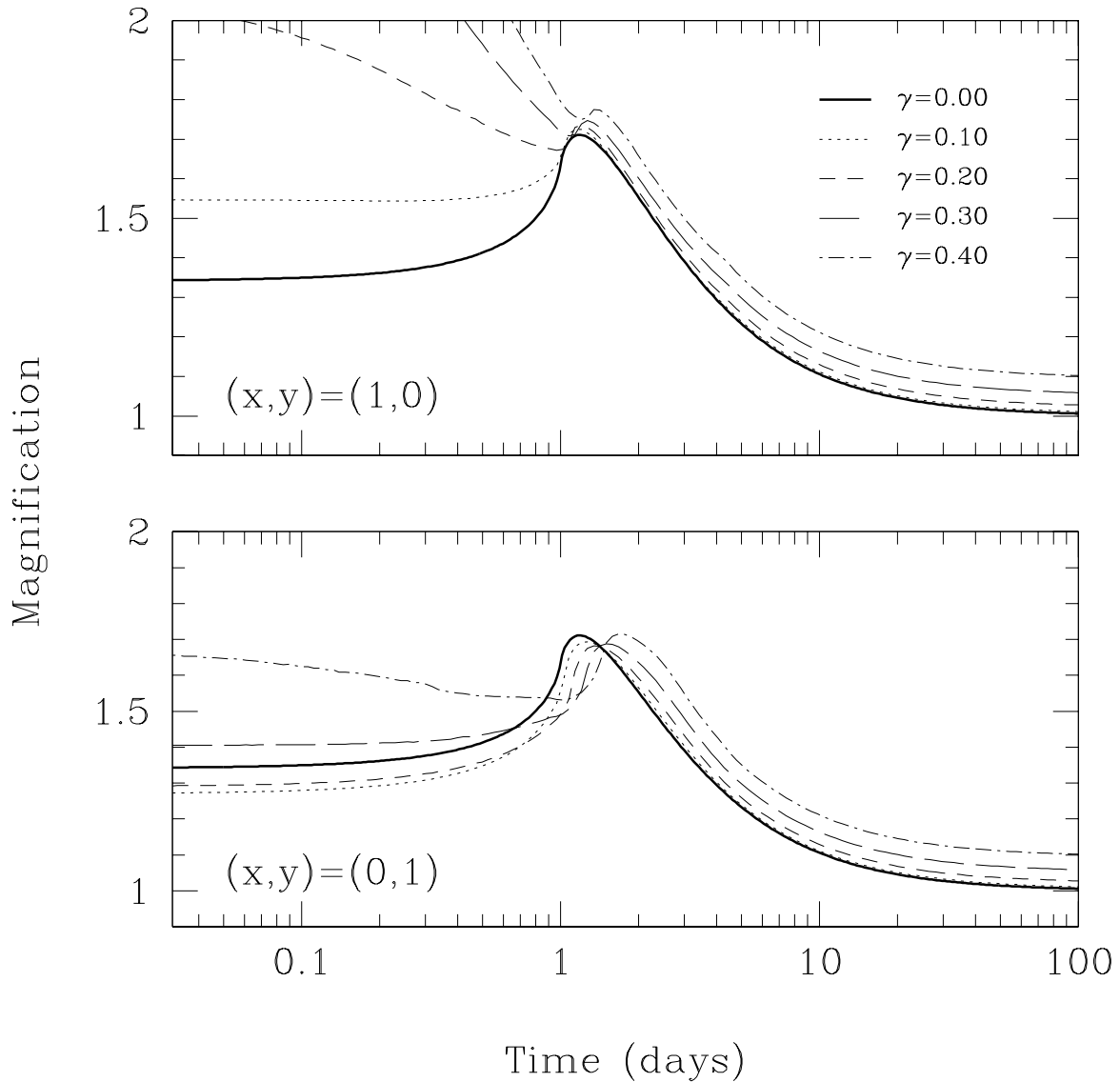


Fig. 4. Magnification as a function of time for a uniform source with $R_0 = 1$ and $b = 1$ for a single lens with external shear along the x-axis of magnitude 2 for various values of γ . Top Panel: Assuming the center of the source is located on the x-axis of the lens. Bottom Panel: Assuming the center of the source is located on the y-axis of the lens.

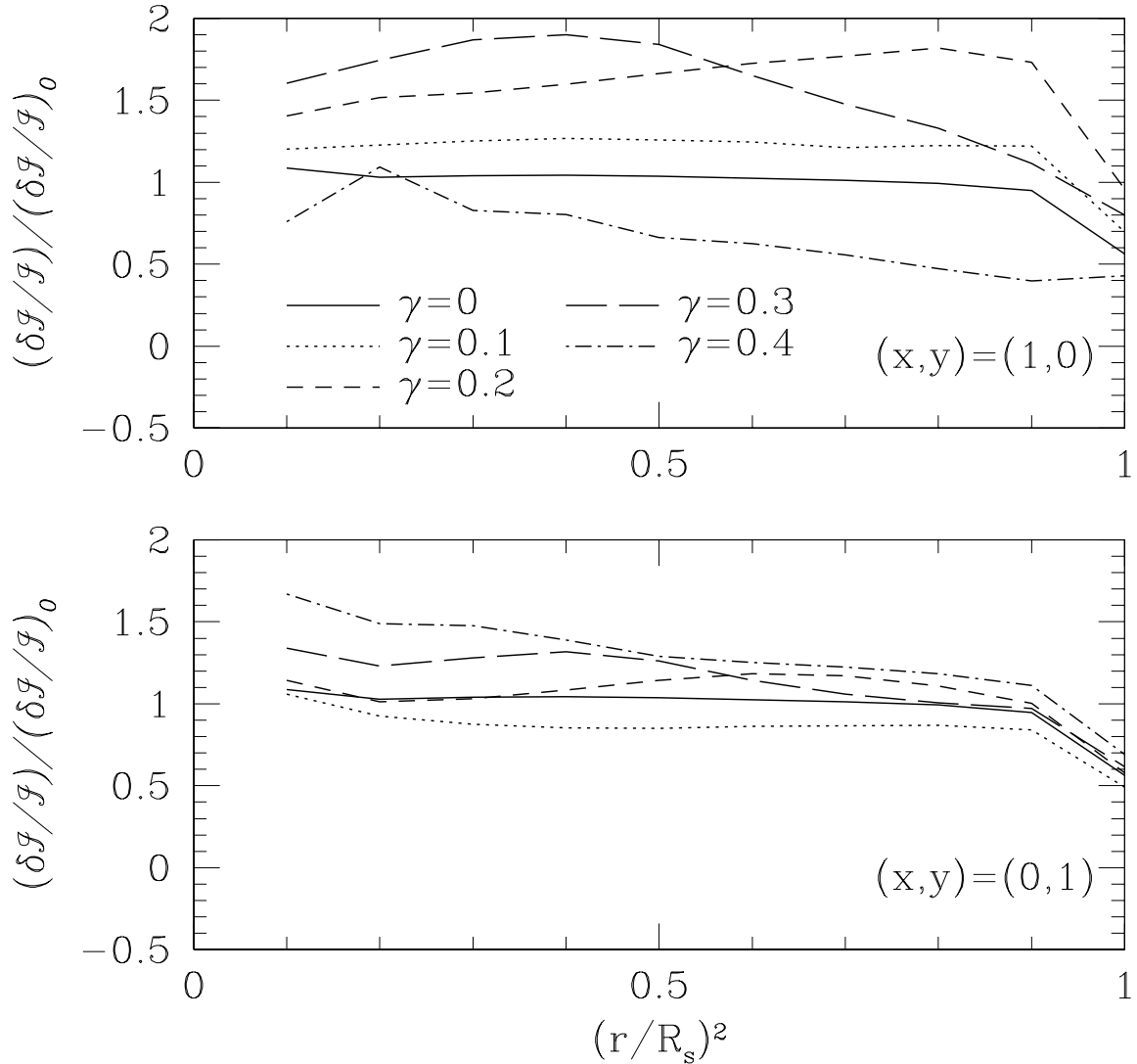


Fig. 5. The fractional error in the recovered intensity profile $I=I$ normalized to that given by the fiducial error ($I=I_0$) given by the scaling relation in equation (13), as a function of the square of the normalized radius $X = r=R_s$ of the afterglow for various values of the external shear along the x -axis. We have assumed $R_0 = 1$, $b = 1$, and a uniform source. Top Panel: Assuming the center of the source is located on the x -axis of the lens. Bottom Panel: Assuming the center of the source is located on the y -axis of the lens.

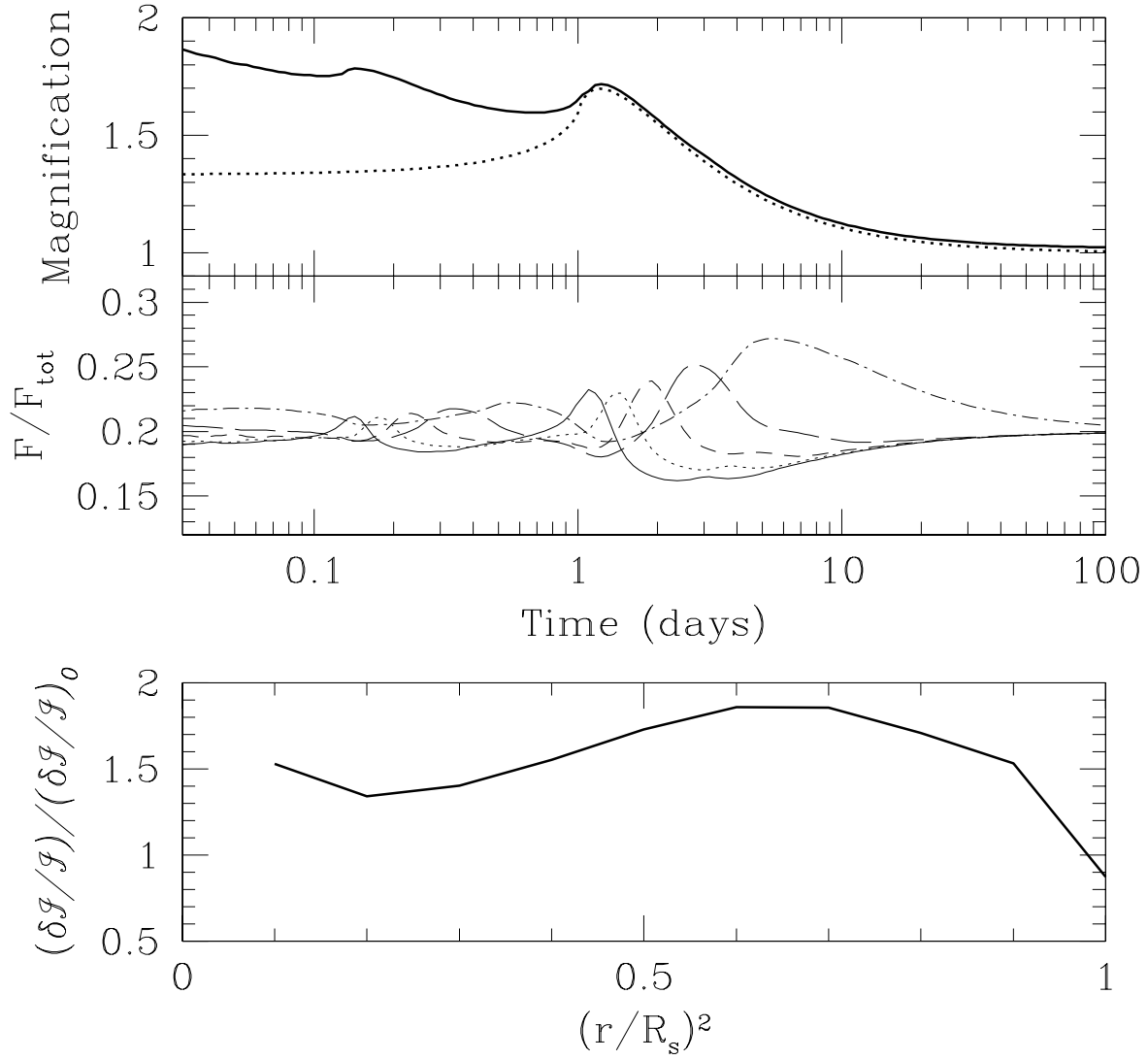


Fig. 6. Top Panel: The magnification as a function of time for a uniform source with $R_0 = 1$. The solid line is for a binary-lens with mass ratio $q = 1$ and a separation of $d = 0.8$ in units of the combined Einstein ring radius. The source is centered on $(0.16, 1)$. The dotted line is for a single lens with impact parameter $b = (0.16^2 + 1^2)^{1/2} = 1.013$. Middle Panel: The fraction of total flux contributed by five equal area annuli as a function of time in days for the binary-lens light curve shown in the top panel. Bottom Panel: The fractional error in the recovered intensity profile $I=I$ norm alized to that given by the ducial error $(I=I)_0$ given by the scaling relation in equation (13), as a function of the square of the normalized radius $x = r=R_s$ of the afterglow.

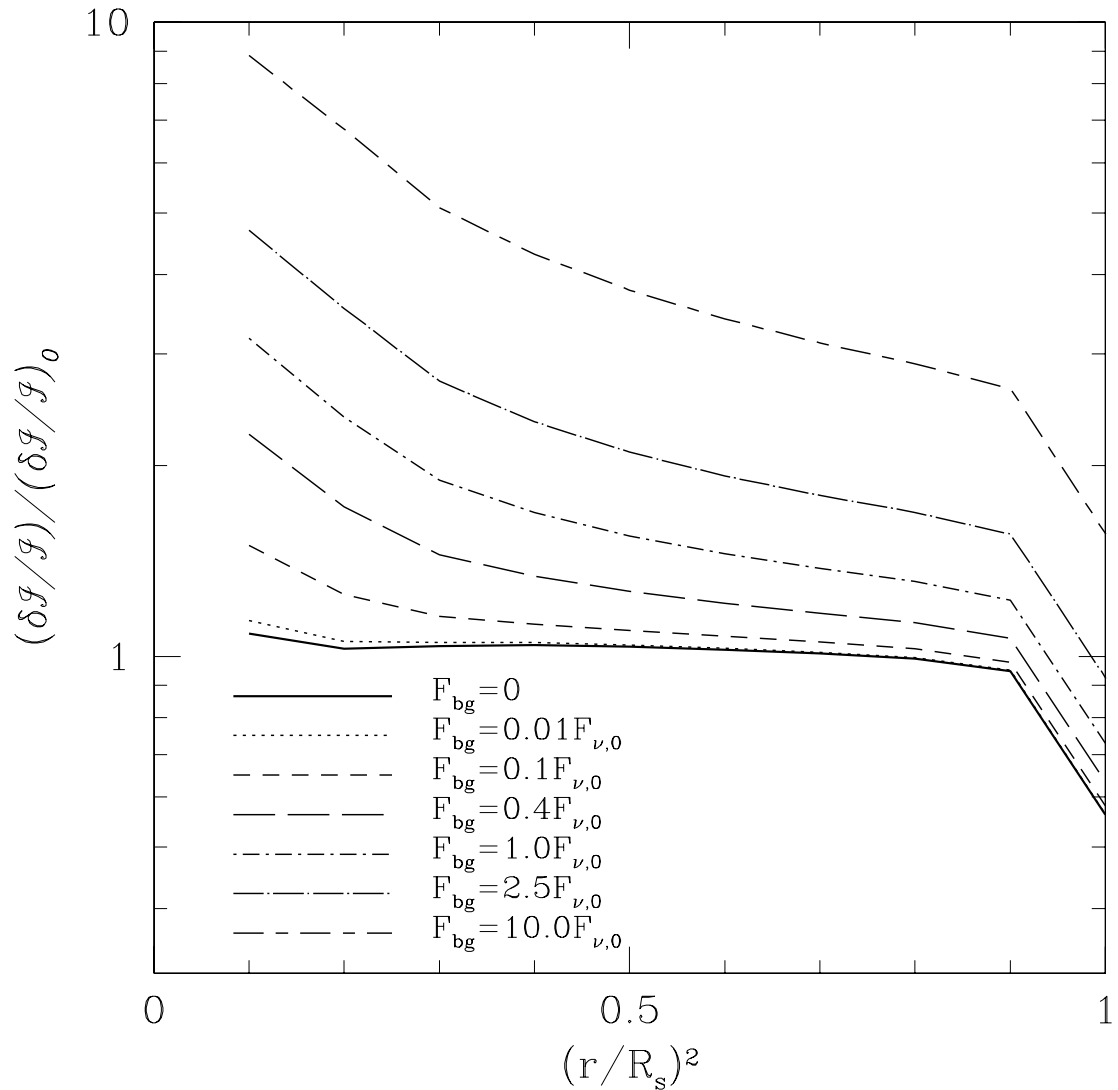


Fig. 7. The fractional error in the recovered intensity profile $I=I$ normalized to that given by the fiducial error ($I=I$) given by the scaling relation in equation (13), as a function of the square of the normalized radius of the afterglow for various assumptions about the magnitude of the unresolved background flux F_{bg} relative to the flux $F_{\nu,0}$ of the afterglow at $t = 1$ day.

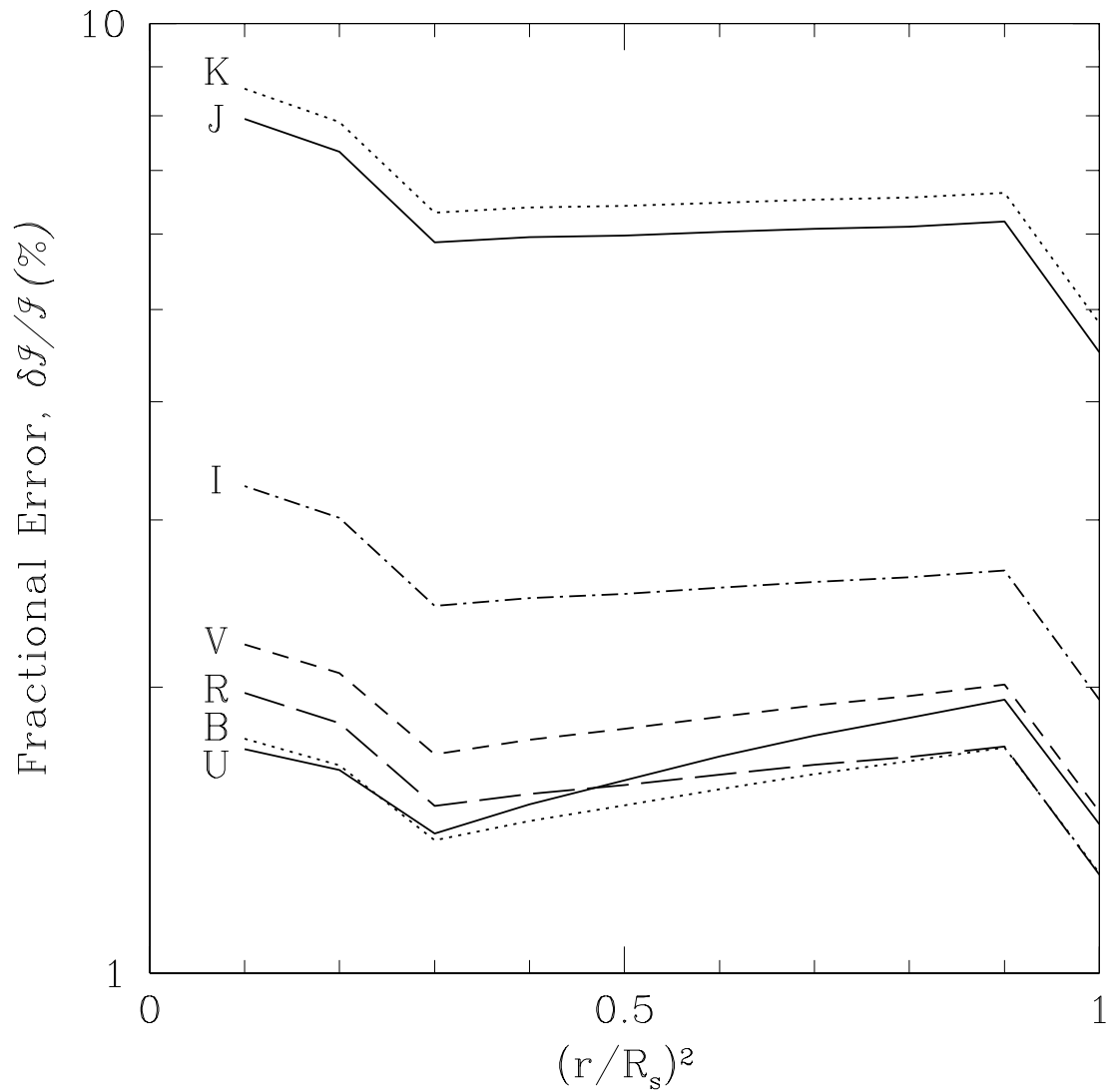


Fig. 8. The fractional error $I = I$ in the recovered relative intensity profile in percent as a function of the square of the normalized radius $X = r/R_s$, for the afterglow and microlensing parameters of GRB 000301C, assuming a uniform source, and that observations were made with a 2 m telescope from the peak of the microlensing event until 30 days after the peak.

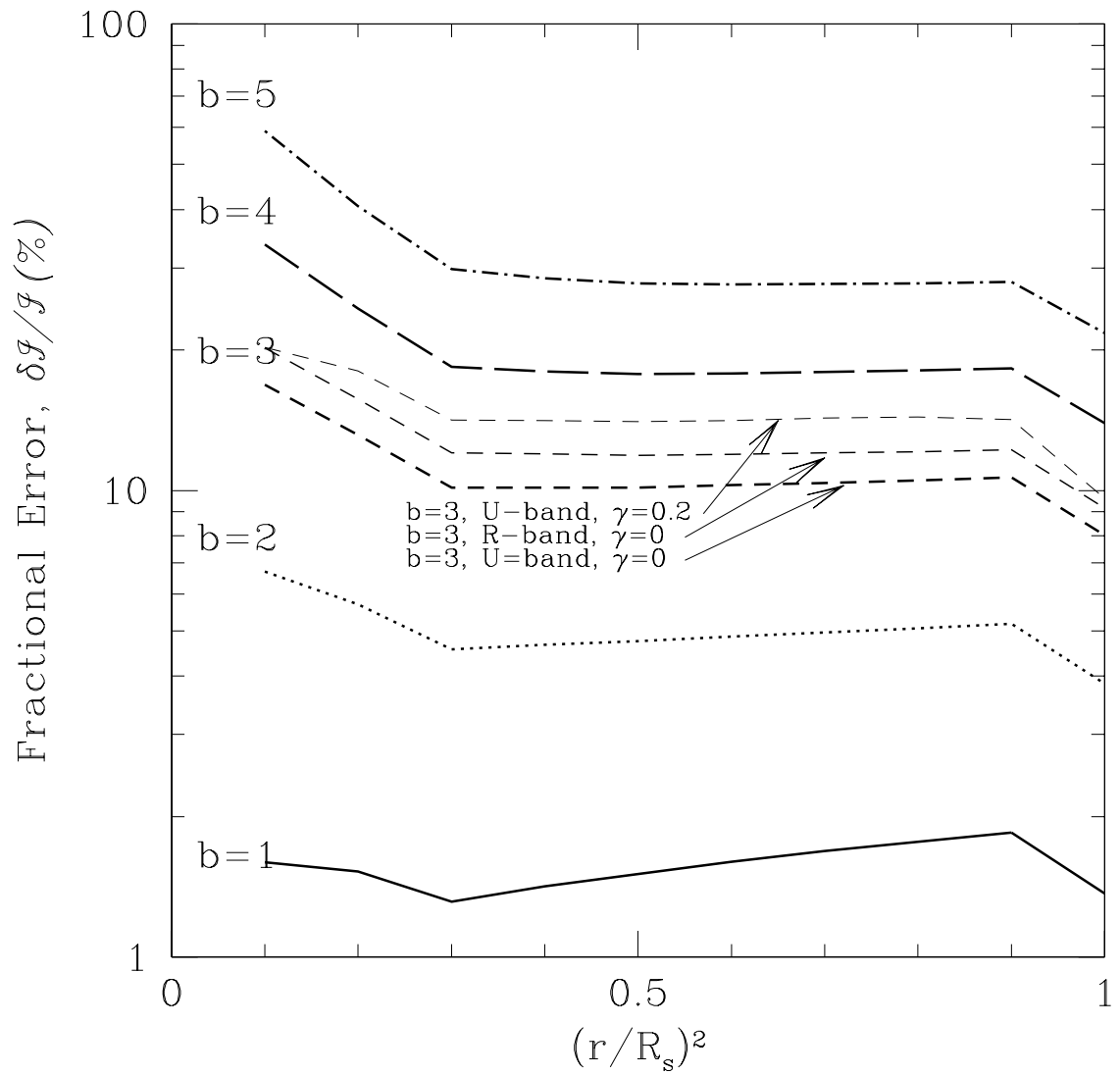


Fig. 9. | Same as Figure 8 for U-band, except we have varied the impact parameter of the microlensing event, b . Note that the fraction of all afterglows with impact parameter b is $1\% b^2$.